SOFT ROBOTICS
Volume 00, Number 00, 2020

DOI: 10.1089/soro.2019.0175

SoRo
Soft Robotics

Twisted-and-Coiled Actuators with Free Strokes Enable Soft Robots with Programmable Motions

Jiefeng Sun,[1] Brandon Tighe,[1] Yingxiang Liu,[2] and Jianguo Zhao[1]

Abstract

Various actuators (e.g., pneumatics, cables, dielectric elastomers, etc.) have been utilized to actuate soft robots. Besides widely used actuators, a relatively new artificial muscle—twisted-and-coiled actuators (TCAs)—is promising for actuating centimeter-scale soft robots because they are low cost, have a large work density, and can be driven by electricity. However, existing works on TCA-actuated soft robots in general can only generate simple bending motion. The reason is that TCAs fabricated with conventional methods have to be preloaded to generate a large contraction, and thus cannot actuate soft robots properly. In this work, an upgraded technique is presented to fabricate TCAs that can deliver 48% free strokes (contraction without preloading). We first compare the static performance of TCAs with free strokes with conventional TCAs, and then characterize how will the fabrication parameters influence the TCAs' stroke and force capability. After that, we demonstrate that such TCAs can actuate centimeter-scale soft robots with programmable motions (gripping, twisting, and three-dimensional bending). Finally, we combine those motions to demonstrate a soft robotic arm that can perform a pick-and-place task. We expect that TCAs with free strokes can enable miniature soft robots with rich three-dimensional motions for both locomotion and manipulation. Because TCAs are electrically driven, we can also potentially develop untethered soft robots by carrying onboard batteries and control circuits.

Keywords: twisted-and-coiled actuator, artificial muscle, programmable motion, soft robots

Introduction

Inspired by biological systems (e.g., octopus), soft robots made from soft materials outperform traditional rigid robots in terms of safety and adaptivity owing to their compliant and deformable bodies.[1] To enable their unique capabilities, soft robots require a key component—the actuator. Many different actuators have been used, including the conventional pneumatic-driven[2] and cable-driven methods,[3] as well as several novel approaches proposed recently such as combustion,[4] dielectric elastomers[5] with variations,[6] chemical reactions,[7] liquid–vapor transition,[8] liquid crystal elastomer,[9] and shape memory alloy.[10,11]

Besides existing actuation approaches, another promising actuator for soft robots is the twisted-and-coiled actuator (TCA), which can be conveniently fabricated by continuously twisting polymer fibers into coiled spring-like shape.[12] Compared with existing actuation methods, TCAs exhibit several unique characteristics: (1) they are low cost since the polymer fibers used to fabricate them can be commonly used household fibers (e.g., sewing threads or fishing line); (2) they have a large work density (27.1 kW/kg),[12] meaning that a TCA can deliver a force much larger than its own weight (generally >100 times)[13]; (3) they can be directly driven by electricity with a small voltage (a few volts)[14]; and (4) they can sense their own deformation through the change of electrical properties (e.g., resistance).[15,16] All of these characteristics will potentially enable small-scale and untethered soft robots that in general are difficult to be accomplished by pneumatic and tendon-driven methods.[17,18] Further, unlike shape memory alloys, TCAs are intrinsically soft, making it possible to embed them in any shape inside a soft body to generate versatile motion.

With the promising characteristics of TCAs, however, TCA-driven soft robots have been scarce. In fact, only several rudimentary soft modules for crawling and bending are

[1]Department of Mechanical Engineering, Colorado State University, Fort Collins, Colorado, USA.
[2]State Key Laboratory of Robotics and System, Harbin Institute of Technology, Harbin, China.

presented in recent years.[19–22] The main reason is that traditional contraction TCAs' large stroke is generally obtained under a preload (e.g., a hanging weight). Without a preload, those TCAs will have negligible strokes because all the coils almost contact with each other. Such preloads will cause problems when TCAs are used to actuate soft robots since a preload will easily deform the soft body due to the low force bearing capability of soft materials (Young's modulus 10^4~10^9 Pa).[1] For example, if we first preload a TCA by applying a stretching force before embedding it into a soft body, the tension force of the TCA will deform the soft body after removing the force. To address this problem, we can use an antagonistic configuration by using two TCAs in parallel, but it will require a larger force to bend, resulting in a small bending range.[23] Note that TCAs that can extend generally do not need a preload, but they can only deliver much smaller forces compared with contraction ones.[24]

In this article, to better actuate soft robots with TCAs, we introduce a novel fabrication technique of contraction TCAs that will have uniform initial gaps between neighboring coils. In this case, they can contract >48% without a preload, termed *free stroke* in this article. Such free strokes can enable soft robots by directly embedding one or multiple TCAs into a soft body without preloading those TCAs (Fig. 1a). With a large free stroke, TCAs can actuate the soft body to achieve a large magnitude of motion. They can also be arranged in different shapes inside a soft body to achieve programmable motions.

The main contributions of this article are twofold. First, we propose an upgraded fabrication method to generate TCAs with free strokes. Such TCAs can be applied to a wide variety of applications that requires artificial muscles, including robotics, haptics, intelligent structures, smart textiles, etc.[25] Second, we demonstrate soft robots with programmable motions by placing TCAs in different shapes inside a soft body. Specifically, we embed TCAs in a curved U shape, a helical shape, and straight shapes in parallel to enable three different motions: two-dimensional bending, twisting, and three-dimensional bending, respectively (Fig. 1b–d). We also combine the three motions to demonstrate a completely soft robotic arm that mimics a human forearm (Fig. 1e, f). Such demonstrations lay a foundation for achieving more complicated motion or shape morphing by strategically embedding multiple TCAs inside a soft body, similar to recent results using other actuation methods (e.g., pneumatic-driven[26] and liquid crystal elastomers[27,28]). We envision that this work will inspire a variety of TCA-driven soft/rigid robots or structures to achieve versatile motions or morphologies, especially those in centimeter scales.

Results and Discussion

TCAs with free strokes

The fabrication process for TCAs with free strokes is built on the original mandrel-coiling process[12,29] with a key difference: we coil a twisted thread on a special mandrel with a helical groove, generating a coiled shape with uniform initial gaps between neighboring coils.

The major steps to fabricate a TCA with free strokes are shown in Figure 2 (details in Supplementary Fig. S1 using our customized machine). First, a conductive sewing thread is twisted to generate a twisted thread with the fiber pitch angle α_f and length l_0 (Fig. 2a). Then, the twisted thread is coiled in the same direction as twisting on the special mandrel with a helical groove that has a coil pitch angle α_m (Fig. 2b). The groove is formed by uniformly wrapping a copper wire around a mandrel core (a cylindrical rod). With the groove, the twisted thread will be guided into a helical shape with gaps between coils. Without the helical groove, the twisted thread will not have gaps because the coils will be pulled together by a pulling force generated by the internal untwisting torque in the thread (Fig. 2b). After the coiling process, the coiled twisted thread is annealed in an oven with the helical mandrel whose two ends are fixed to set this shape as an equilibrium state (Fig. 2c). After annealing, the coiled twisted thread can be removed from the helical mandrel to generate a final TCA. A training process (several slow heating cycles) needs to be applied before the first-time use to remove the TCAs internal stress to get consistent performance.[12]

Using the proposed procedure, we fabricate five different TCAs according to two important fabrication parameters (details in Supplementary Table S1): pitch angle during coiling (α_m equals the pitch angle of the helical groove) and annealing temperature (T_a). We choose the pitch angle because it will influence the initial gaps l_g between neighboring coils (Fig. 2b). In fact, $l_g = 2\tan(\alpha_m)(d_m + d_0)$, where d_m and d_0 are, respectively, the diameter of the mandrel core and the twisted thread (Figs. 2b and 3a). The annealing temperature will influence the dynamic response of TCAs as will be presented in the next subsection. Note that we choose these two factors because other fabrication parameters are easy to interpret or have been characterized by others (e.g., the number of plys, the number of rotation inserted, the spring index, and different materials[12,30]). We categorize the four TCAs according to the pitch angle α_m. For Type 1, $\alpha_m = 15.57°$, and Type 2, $\alpha_m = 22.54°$ (see Supplementary Table S1 for detailed fabrication parameters). For each type, we anneal them under two temperatures (180°C and 200°C) and use a number after type number to indicate the temperature. For example, Type 1-180 is annealed at 180°C, whereas Type 1-200 is annealed at 200°C.

Each of the four TCAs has initial gaps between adjacent coils (Fig. 3a, b) that allow free strokes without preloading. Each TCA exhibits a *natural length* l_n at room temperature when no load is applied. It can achieve a minimum length l_{min} when heated, which is the length when all coils contact (Fig. 3b). Therefore, the TCA can generate a reversible *free stroke* $S_f = (l_n - l_{min})/l_n$ without a preload.

To demonstrate the free stroke, we actuate our TCAs using electricity to drag a weight placed on a PVC sheet (Fig. 3c). The results show that a single TCA (Type 2-200 in Supplementary Table S1) that weighs only 0.03 g can overcome a peak friction force of 0.4 N to achieve a free stroke of $S_f = 48\%$. By using five TCAs (weigh only 0.16 g) in parallel, we can drag a coffee kettle of 2 kg to move 60 mm (Supplementary Video S1). The maximum force that the TCA can generate before breaking is 0.78 N (stress 8.59 MPa) when the two ends are fixed under the natural length.

Our TCAs can also be used when a preload is applied (Fig. 3d) similar to conventional TCAs without free strokes. In this case, the stroke is defined as $S = (l_{\text{load}} - l_{min})/l_{\text{load}}$, where l_{load} is the TCAs' length after a load is applied. Results show that our TCA (Type 2-200) can generate a stroke of 55% under 10 g load (Fig. 3d and Supplementary Video S2).

We compare our TCAs with several representative works[12,22,23,30–35] in Table 1 by categorizing them based on

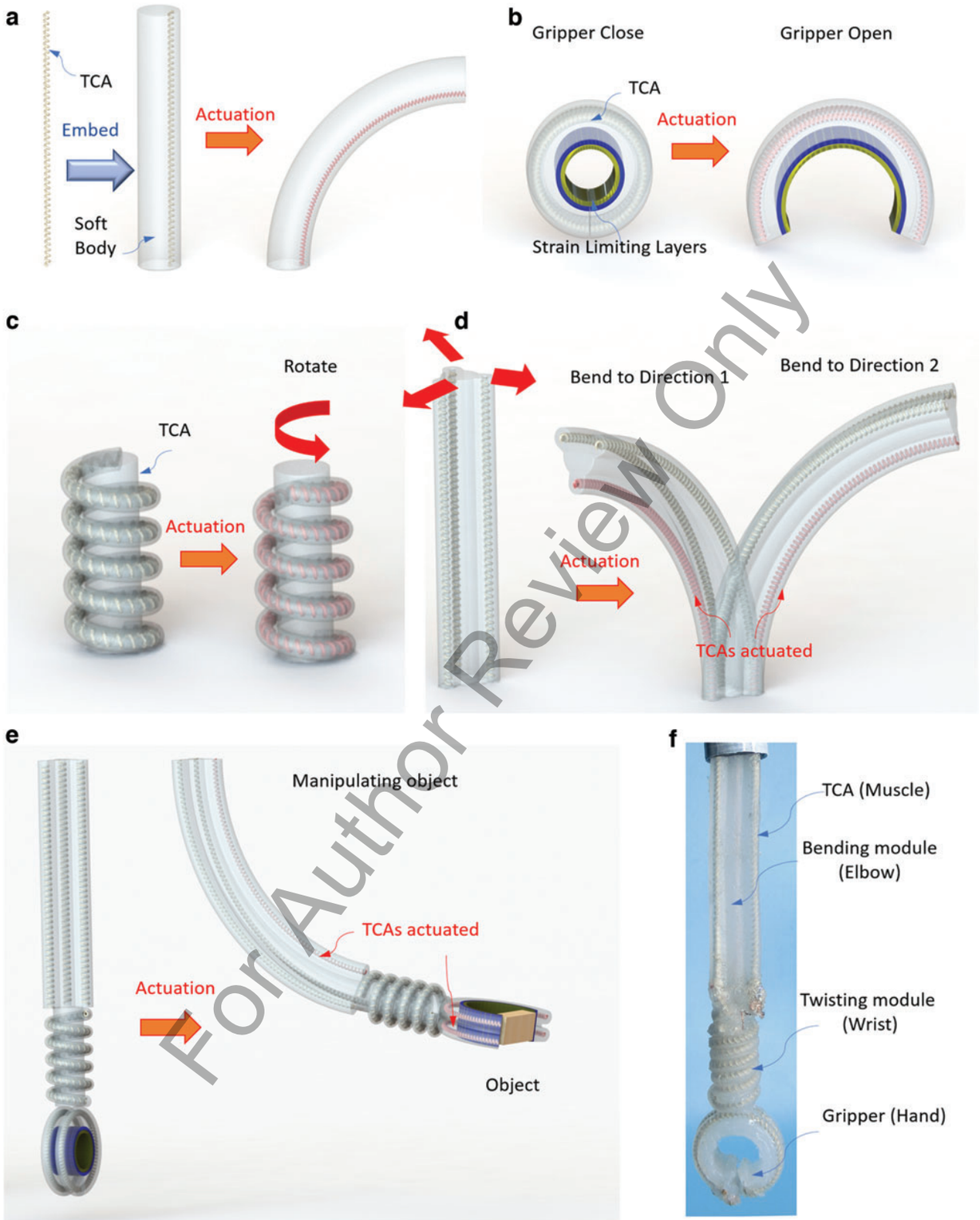

FIG. 1. TCAs with free strokes can enable programmable motions for soft robots. **(a)** TCAs with free strokes can be directly embedded into a soft body to generate a large bending angle when actuated. **(b–d)** Versatile motions generated by arranging TCAs in soft bodies. **(b)** A 2D bending module (gripper) with TCA in a curved U shape. **(c)** A twisting module with a TCA in a helical shape. **(d)** A 3D bending module with three TCAs in parallel. **(e)** The schematic of a soft robotic arm with a 3D bending module, twisting module, 2D bending module. **(f)** A prototype of the soft robotic arm. TCA, twisted-and-coiled actuator. Color images are available online.

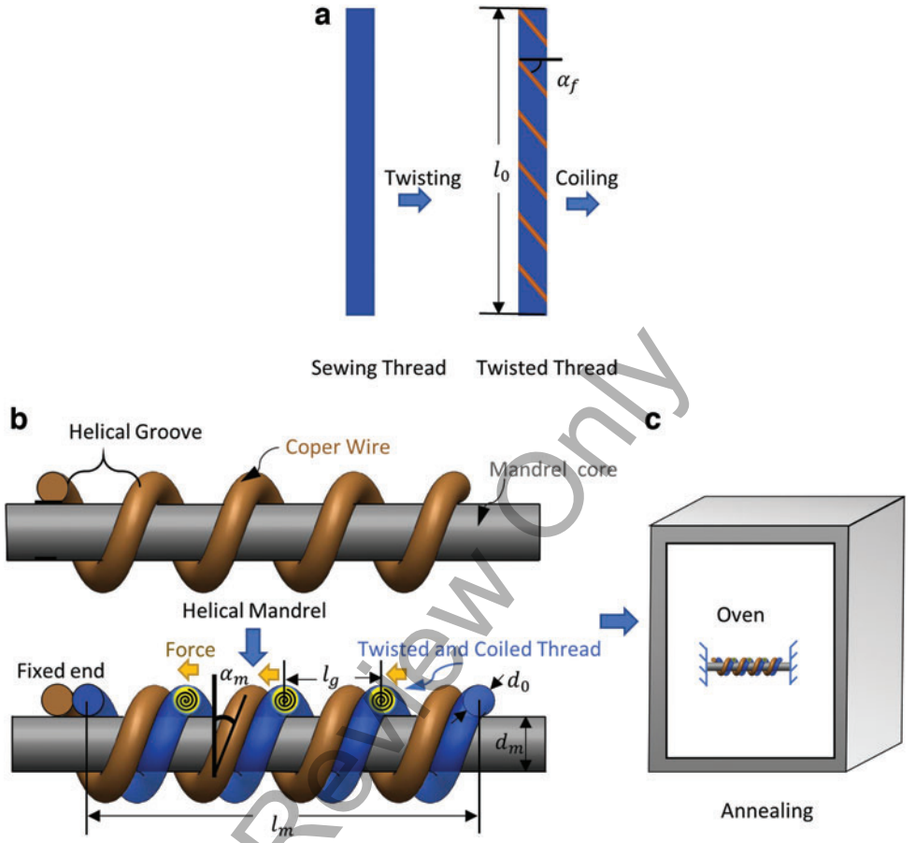

FIG. 2. The schematic showing the fabrication process of TCAs with free strokes. **(a)** Twist a sewing thread to generate a twisted thread. **(b)** Coil the twisted thread on a helical mandrel with a cylindrical mandrel core and helical grooves formed by a copper wire to generate coiled and twisted thread. **(c)** Anneal the coiled and twisted thread in an oven to generate the final TCA. Color images are available online.

the coiling method: self-coiling (twist-induced coiling) and mandrel coiling. In general, most of the existing TCAs have negligible free strokes because the coils contact with each other after fabrication. For the strokes with preload, the largest stroke using the mandrel-coiling method is 53%,[23] and the largest stroke using the self-coiling method is 45%.[35] The stroke marked with a in Table 1 indicates that the stroke is normalized by l_n instead of l_{load} and will become smaller when normalized with l_{load}.

Characterization of TCAs with free strokes

In this section, we experimentally characterize TCAs with free strokes through two steps. First, we obtain the static response with respect to temperature and compare the results with traditional TCAs without free strokes. We also explain the results using a model developed with the system identification method. Second, we experimentally investigate dynamic response with respect to time for the four TCAs with free strokes to choose one that will be suited for actuating soft robots.

Static response with respect to temperature. To see why TCAs with free strokes are better than traditional TCAs, we fabricate a traditional TCA using a mandrel without the helical grove: Type 0-180. We compare its static response with Type 1-180 with free strokes. To make proper comparisons, these two TCAs are made from the same twisted thread with the same parameters (details in Supplementary Table S1).

For these two TCAs, we perform static experiments by hanging a weight at the end of each TCA, slowly increasing the TCAs' temperature in an oven, and recording the displacement (see Supplementary Fig. S2 for details). Three TCAs that are separately fabricated are tested, and their performance is pretty consistent because our TCA is fabricated with a customized, highly automatic machine. Therefore, only one TCA for each type is used throughout the systematic characterization. In the experiments, one experiment is repeated three times. Only the average of the three experiments is plotted in the following for a clear view and easy comparison, and the maximum standard deviation of all experiments (in Figure 4a to c) is 2.14 mm. The detailed measurement uncertainty (standard deviation) is reported in Section 5 of the Supplementary Data.

Experimental results of displacement with respect to temperature are plotted in Figure 4a for three different hanging weights: 0, 20, and 40 g. From the results, we can observe that all curves almost overlap with each other at the beginning, indicating that they can be actuated similarly when the temperature is relatively low (<70°C) as observed previously by Haines *et al.*[12] and Kianzad *et al.*[36] However, all curves will flatten out as the temperature becomes high, suggesting that the coils in TCAs are contacting each other to prevent further contraction. For different TCAs with the same weight, Type 1 can generate a larger displacement than Type 0, and the difference becomes larger as the weight increases. For instance, with 0 g (from 25°C to 150°C), Type 0

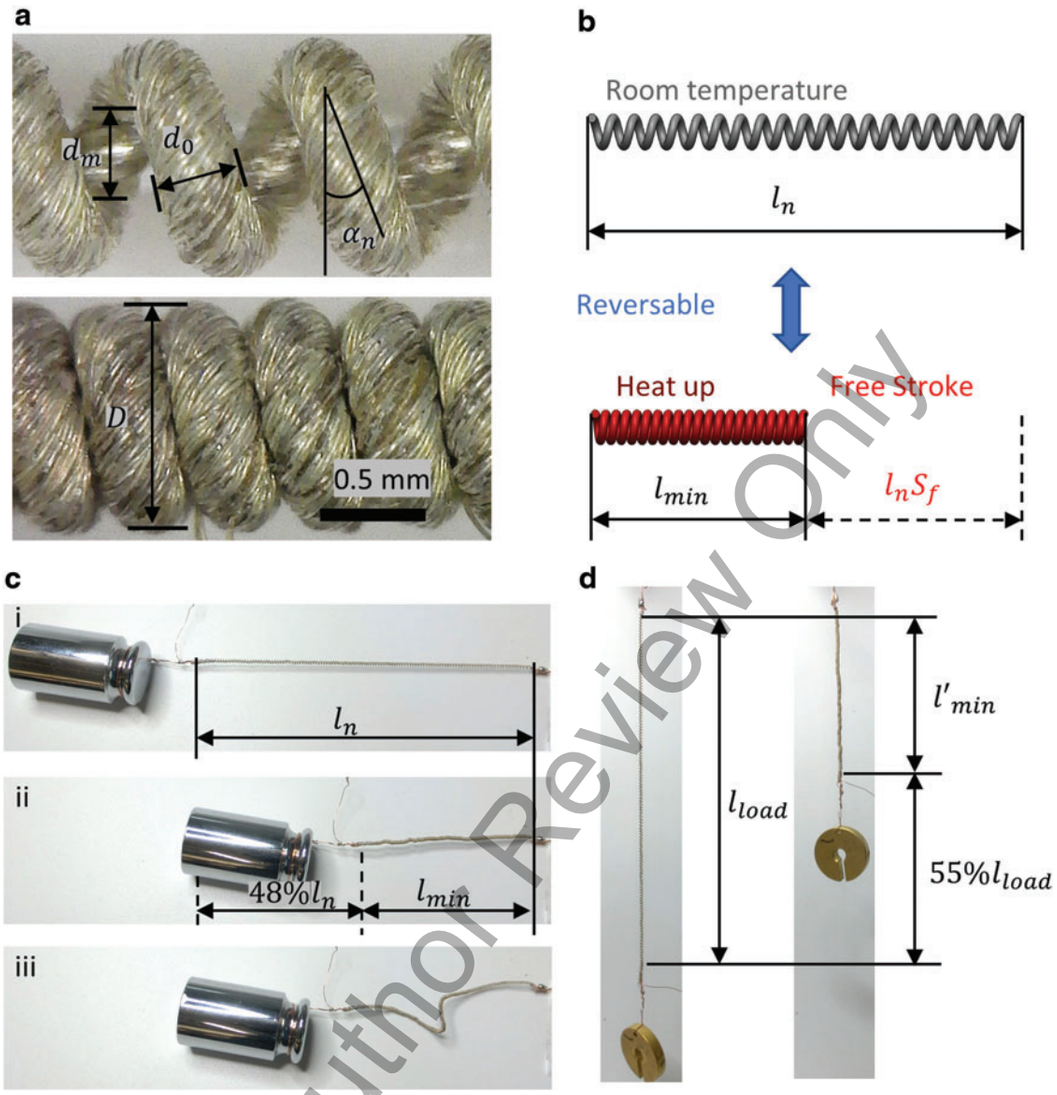

FIG. 3. Our proposed TCAs can contract without preloading. **(a)** Microscopic photographs of the TCA in room temperature (*top*) and after being heated up (*bottom*). **(b)** Schematic of the TCA illustrating natural length l_n, minimum length l_{min}, and the free stroke S_f. **(c)** The TCA pulls a weight against friction of 0.4 N to generate a free stroke of 48%. (i) The TCA is in its natural length; (ii) The TCA is actuated to contract to its minimum length; (iii) The TCA automatically extends and recovers to its natural length after cooling down. **(d)** The TCA lifts a weight of 10 g against gravity to generate a loaded stroke of 55%. l'_{min} is the minimum length of the TCA when a weight is hanged at the end and will be longer than l_{min} which is the minimum length of the TCA when no weight is hanged. Color images are available online.

can contract 4 mm, while Type 1-180 can contract 20 mm. Note that Type 0 seems to contract >4 mm because the length of the TCA falls below the minimum length due to curling of its shape. But with 40 g (from 25°C to 150°C), Type 0 can contract only 24 mm, while Type 1-180 can contract 44 mm. For the same TCA under different weights, the case with the largest weight generates the most contraction since a heavier weight causes more gaps between coils (see Supplementary Fig. S3).

To better explain the difference between the traditional TCA and TCAs with free strokes, we can use a mathematical model to describe the relationship between temperature and the displacement[37]:

$$F = k(l - l_n) + c\Delta T, \tag{1}$$

where F is the external load, k is the stiffness coefficient of the TCA, c is the force–temperature coefficient, l is the TCAs' length, $\Delta T = T - T_0$ is the increase of temperature with T and T_0 the TCAs' current and room temperature, respectively.

We can rearrange Equation (1) to obtain the length in terms of temperature change:

$$l = -\lambda\Delta T + l'_n,\ l \geq l_{min}, \tag{2}$$

where $\lambda = c/k$, and $l'_n(m) = F/k + l_n = mg/k + l_n$. We can use this equation to explain the performance difference for

Table 1. Comparison of Twisted-and-Coiled Actuators' Strokes with Representative Works

Reference	*Precursor fiber*	*Coiling*	*Spring index*	*Free stroke*	*Stroke, %*	*Load for stroke*
Haines *et al.*[12]	Fishing line	Mandrel	5.1	NA	49	1 Mpa
Haines *et al.*[30]	Fishing line	Flat spiral	NA	NA	46	NA
Wu *et al.*[23]	Fishing line	Mandrel	5.2	NA	53	100 g (1.8 Mpa)
Li *et al.*[31]	Fishing line	Self-coiling	NA	NA	18[a]	100 g
Yip *et al.*[32]	Conductive thread	Self-coiling	NA	NA	10	200 g
Cho *et al.*[33]	Conductive thread	Self-coiling	NA	NA	17.8	1000 g
Almubarak *et al.*[22]	Conductive thread	Self-coiling	NA	NA	22[a]	200 g
Kim *et al.*[34]	Spandex and conductive thread	Self-coiling	NA	NA	40.1	1.9 N
Yang *et al.*[35]	Spandex	Self-coiling	NA	NA	45	60 g
Our work	Conductive thread	Helical Mandrel	3.5	48%	55	10 g

[a]Normalized by l_n instead of l_{load}.

conventional TCAs and TCAs with free strokes in two different cases. First, when $F = 0$, the convention TCA almost cannot contract anymore since $l'_n = l_n \approx l_{min}$. But for TCAs with free strokes, $l'_n = l_n > l_{min}$, there will be a free stroke, and it will contract to l_{min} at a higher temperature. To see this, we plot the length with respect to temperature for the two TCAs in Figure 4b and c (figures with shaded error bars can be found in Supplementary Fig. S4a, b). We also label the l_n and l_{min} in the figure. In these two figures, the blue shaded area indicates the amount of the free stroke, and the TCA with

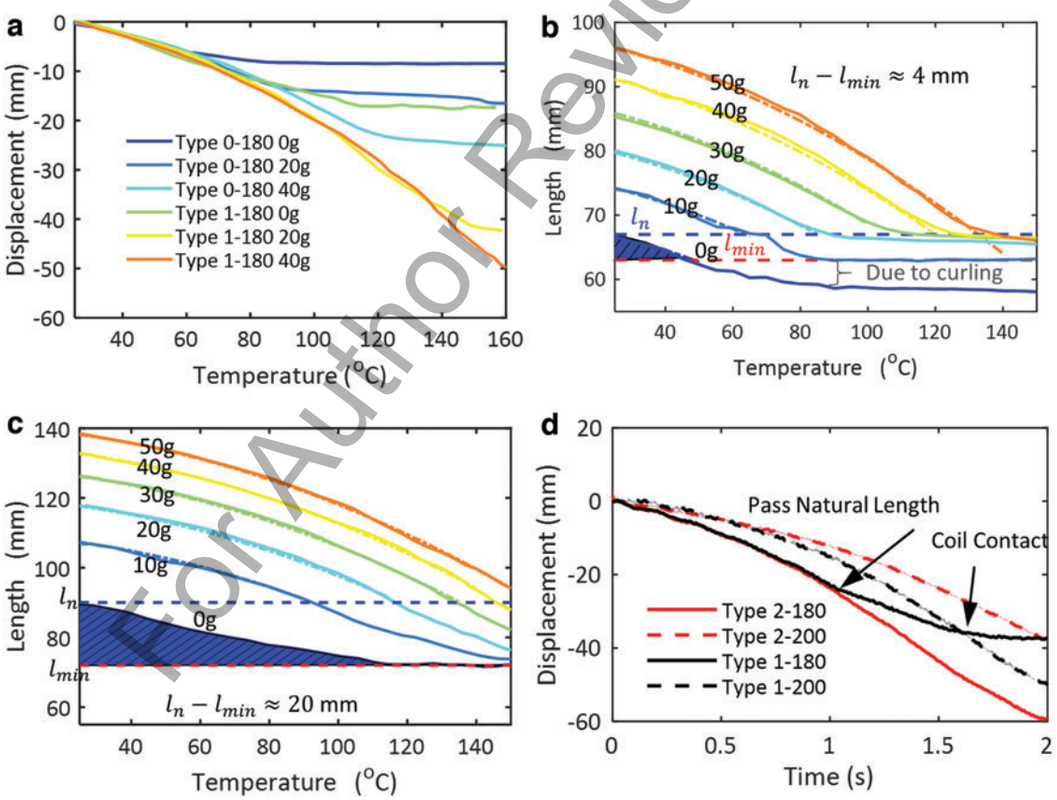

FIG. 4. Characterization of the static response with respect to temperature for a conventional TCA (Type 0) and a TCA with free strokes (Type 1). **(a)** The displacement with respect to temperature under different weights. **(b)** The experimental (*solid lines*) and fitted (*dash-dotted lines*) results of a conventional TCAs (Type 0) length with respect to temperature. **(c)** The experimental (*solid lines*) and fitted (*dash-dotted lines*) results of the TCAs (Type 1) length with respect to temperature. The figures with *shaded* error bars can be found in Supplementary Fig. S4a and b of the Supplementary Data. **(d)** The dynamic response with respect to time for four different TCAs with free strokes when actuated by a constant current (1 A) under the same load (20 g). Type 2-180 (*red solid line*) responds faster with a large displacement. The *lines* indicate the average, and *shaded* regions indicate the standard deviation. The maximum standard deviation for the four curves is 2.12. Color images are available online.

free strokes can access a larger shaded area compared with the conventional TCA. Second, for a fixed weight (i.e., $F \neq 0$), $l'_n(m) = F/k + l_n$ will be larger for a TCA with free strokes since its k will be smaller under the same fabrication conditions. In this case, TCAs with free strokes can also generate larger displacements as can be seen from the five curves corresponding to 10, 20, 30, 40, and 50 g in Figure 4b and c. We also approximate λ using a polynomial $\lambda = a\Delta T + b$ in terms of temperature, and plot the fit results as dash-dotted lines, which match well with experimental results (see Section 5 of the Supplementary Data for details). However, the model does not capture the plateau part of the experimental data; therefore, it can only be used to predict the first part of the actuation. A more sophisticated model could be developed by considering the contact of coils.

Dynamic response with respect to time. The static response for TCAs with free strokes indicates that the displacement largely depends on the pitch angle during coiling (α_m). Besides static response, we characterize how the annealing temperature will influence TCAs' dynamic performance, which is critical if we want to rapidly actuate soft robots, as most current TCA-driven soft robots are in general relatively slow. For example, a soft bending module can only bend 60° after 10 s actuation, and a crawling robot can only move 1.2% of its body length per second[19,20] while the crawler actuated by shape memory alloy wire can move >200% of its body length per second with a rolling gait.[38] For a given length of twisted thread l_0 in Figure 2a and b, a TCAs' length after removing from the mandrel after annealing is around $l_m = l_0 \sin \alpha_m$. We call l_m the made length. But in general the natural length $l_n \leq l_m$ depending on the annealing temperature (T_a).

If T_a is below the Brill transition temperature of Nylon 6,6 (160°C),[39] the TCAs, after removing from the mandrel, will automatically reduce its length until all gaps disappear to a minimum length given a sufficiently long time (several days) or subjected to a few heating cycles—a process called creep, which has also been observed by others.[39] When T_a is >160°C and <200°C, the TCA will automatically creep to a natural length that is longer than its minimum length but shorter than the made length. For example, the natural lengths of Type 1-180 and Type 2-180 TCA are 92.5% and 80.5% of their made lengths (Supplementary Table S1), respectively. The reason is that when the annealing temperature is low (e.g., <200°C), the annealing process cannot fully remove the stress in the twisted thread. However, the TCAs annealed at 200°C can almost maintain the made length (Supplementary Fig. S3, weight = 0). Therefore, the TCAs' natural length will not only depend on the pitch angle during coiling, but also on the annealing temperature that determines the extent to which the TCA can hold the designed shape.

With the four TCAs with free strokes, we experimentally characterize their dynamic response under a constant weight (20 g) by applying a constant current (1 A) for 2 s to determine which one is better for actuating soft robots. Since these TCAs are fabricated with precursor threads of the same length, and thus resistance, they almost have the same temperature at the same time in the experiment. Figure 4d plots the displacement with respect to time, and the maximum standard deviation for the four curves is 2.12 mm, <4% of the TCAs' maximum displacement (60 mm). The results suggest that a TCA with $T_a = 200$°C (dash lines) can have a larger natural length, thereby a longer displacement upon actuation, but it has a slower time response compared with TCAs fabricated with $T_a = 180$°C. In other words, TCAs annealed at 180°C (solid lines) can generate faster motion under the same actuation power compared with the TCA annealed at 200°C (dash lines). When we focus on the TCA annealed at 180°C, we observe that Type 1-180 TCAs contraction speed drops at a certain point, and its final displacement after 2 s is less than Type 2-180 TCA (red solid line). The reason is that it passes the natural length since Type 1-180 TCA has a shorter natural length than Type 2-180 TCA. Among the four types of TCAs, Type 2-180 TCA (red solid line), which is annealed at a lower temperature but with a longer made length, is a better candidate for actuating soft robots since it actuates faster with a large displacement.

We also observe a *temporary natural length* due to the creep (viscoelasticity) of Nylon 6,6, the material of the threads used for fabricating TCAs with free strokes. Such a phenomenon is also mentioned in Refs.[40,41] for TCAs made of fishing lines. When a load is hanged at the end of a TCA, the length of TCA will first instantly increase due to the elastic stiffness of the spring structure and then gradually increase over time (Supplementary Fig. S5b). After a TCA creeps to one length induced by a load, it takes a pretty long time in room temperature to return to its natural length after the load is removed (see Supplementary Data for more explanations and experimental verification). If a TCA is embedded into a soft body in these temporary natural lengths after the fabrication process, it will eventually recover to its natural length, which will cause undesired initial deformation of the soft body. Therefore, we first conduct one heating cycle (in addition to the training process) before embedding the TCA into a soft body to prevent the undesired deformation. Also, we tested the ''aging'' of the TCA (Type 1-180) by actuating it for 10,000 cycles (0.25 Hz) at 2 MPa load, and the results show that the stroke changes little (2% as shown in Supplementary Fig. S6 more details in Section 7 of the Supplementary Data). The viscoelasticity might be also the reason for the hysteresis during actuation, and more sophisticated treatment can be found in other references.[42,43]

TCA-actuated soft robots with programmable motions

The inherent softness of TCAs allows us to embed it with an arbitrary shape inside a soft body to generate programmable and versatile motions. To demonstrate this, we embed TCAs in a curved U shape, a helical shape, and straight shapes in parallel to enable three different motions: two-dimensional bending, twisting, and three-dimensional bending, respectively. These three motions represent typical ways to arrange soft artificial muscles in a 3D shape within a soft body to achieve complex motion. Further, they can be combined together to generate a soft robotic arm that mimics a human forearm to perform pick-and-place tasks (see Combination of Modular Motions: A Soft Robotic Arm section). For the results presented below, we only use the same module throughout the experiments (the soft robotic

arm comprises the same module used in the characterization sections) to maintain consistency.

Two-dimensional bending. We demonstrate two-dimensional bending motion with a soft gripper that is initially closed and can be opened by actuating an embedded TCA (Fig. 5a). We choose such a design strategy because the gripper can hold an object without consuming additional energy, whereas traditional soft grippers need to continuously consume energies when holding an object.[24] Further, our design only requires a single TCA, simplifying the design and eliminating possible complicated position control for grasping.[44]

The gripper is made of four parts: a curved U-shaped TCA (total length: 70 mm), a straight soft body (size: $35 \times 3 \times 5$ mm), one elastomer layer stiffer than the soft body, and one stretched (120%) elastomer layer (Fig. 5a). The soft body has two through holes to host the U-shaped TCA to generate uniform bending. The elastomer layer without prestretch serves as a strain limiting layer, while the one with prestretch bends the soft body to generate an initially closed shape. Such a fabrication allows us to avoid the difficulty to create channels with spatially curved U shape (see Supplementary Fig. S7 for fabrication details).

To effectively use the proposed gripper for grasping objects with different sizes and weights, we need to address two questions: (1) how to open to different widths (d_w in Fig. 5b), so that it can grasp objects with different sizes; (2) how to determine the gripping force (F_g in Fig. 5c) it can generate at a given open width to make sure it can hold an object without additional energy input. We experimentally address these two questions. First, we evaluate how d_w will change with respect to the applied power for a fixed amount of time (2 s). The results shown in Figure 5b (also Supplementary Video S3) indicate that d_w increases with respect to the input power, and the slope of the curve increases because the TCA displaces longer in the higher temperature region than in the low-temperature region as shown in Figure 4d. To determine the gripping force, we drag the gripper open and record the displacement and force. Results in Figure 5c suggest that F_g increases with respect to d_w, which means that a larger opening will allow the gripper to hold a heavier object. The almost linear shape for the gripping force with respect to the opening width can be explained by possible analytical solution $w_d = cF_g$, where c is the constant determined by the geometry and material stiffness (assumed linear within a small range of deformation).[45]

The experimental results shown in Figure 5b and c (the maximum standard deviations are, respectively, 0.7990 mm and 0.085 N) can be used for guiding the grasping of an object. For an object with a given size and weight, we can first determine if it is possible to hold it using results in Figure 5c (given a rough estimation of the friction coefficient). If it is possible to hold it, we can use the results in Figure 5b to apply a proper power to open the gripper to a width that is slightly larger than the object's size. An example grasping process is shown sequentially in Figure 5d with a screwdriver. The gripper can also grasp different objects (a printed circuit board, a screw, and a DC motor) with a variety of sizes and weights owing to the softness of the gripper (Fig. 5e and Supplementary Video S3).

Twisting. To enable twisting motion, we wrap a TCA in a helical shape around a cylindrical soft body (Fig. 6a). Before wrapping, the TCA is first inserted into an elastomer tube to protect the TCA. We investigate two wrapping strategies using TCAs with the same total length (Fig. 6b) to compare the twisting results: a single and double helix. A single helix is obtained by wrapping a TCA uniformly along the soft body, while a double helix is fabricated by folding the TCA in half before wrapping it on the soft body (see the Supplementary Data for fabrication details). To make the twisting module compact (short), we wrap the TCA in both cases as close as possible.

To characterize the twisting motion, we record the twisting angle (ϕ) with respect to time by applying the same power on the two different twisting modules (Fig. 6c), as well as different power for the same amount of time (Fig. 6d). For the results shown in Figure 6c, the constant power is chosen as 28 W, so that the double helix module can rotate $\sim 180°$ in 2 s (Supplementary Video S4). The final twisting angle (ϕ) of the two designs gradually increases with respect to time. As shown in Figure 6c and d (the maximum standard deviations are both 6.3640° for the two figures), the double helix one can rotate faster and realize a larger angle than the single helix one under the same energy input (i.e., same actuation power for the same amount of time). This is because the force generated by the double helix is almost twice the single helix for the same energy input due to the small difference in their averaging wrapping angle (<10°). So the single helix module is limited by the force instead of displacement that a TCA can generate.

Three-dimensional bending. We can also achieve three-dimensional bending motion by placing three TCAs in parallel through three channels in a cylindrical soft body (Fig. 7a and Supplementary Video S5). By properly actuating the three TCAs, we can bend the soft body toward a specific direction (bending direction γ) with a specific amplitude (bending angle θ, Fig. 7b). To characterize how will γ and θ change with respect to the input power for the three TCAs, we choose to apply different powers to TCA1 and TCA2 since other combinations will be similar (TCA1 and TCA3, TCA2 and TCA3). The bending direction γ will be determined by the ratio of powers applied to TCA1 and TCA2, while bending angle θ will be determined by the magnitude of powers applied to TCA1 and TCA2. Therefore, we perform two sets of experiments. In each set, we fix the power applying to TCA2 P_2, while change the power applied to TCA1 P_1, thereby changing the power ratio P_1/P_2. For the first set of experiments, $P_2 = 0.2$ W, and the ratio P_1/P_2 changes from 1 to 5, while for the second set, $P_2 = 0.4$ W, and P_1/P_2 varies in the same range.

To obtain γ and θ, we use a motion tracking system (Trio v120; OptiTrack) to track the end position of the 3D bending module (marker 2, Supplementary Fig. S8). In the simplest case, we can assume the module has a constant bending curvature $\kappa = 1/r$ due to the relatively small weight at the end. In this case, γ and θ can be solved from the end position of the module through the following minimization problem[46]:

$$\begin{aligned} &\min f(\gamma, \theta) = ||p - p'||, \\ &s.t.\ \gamma \in [0, 90],\ \ \theta \in [0, 180] \end{aligned} \tag{3}$$

where

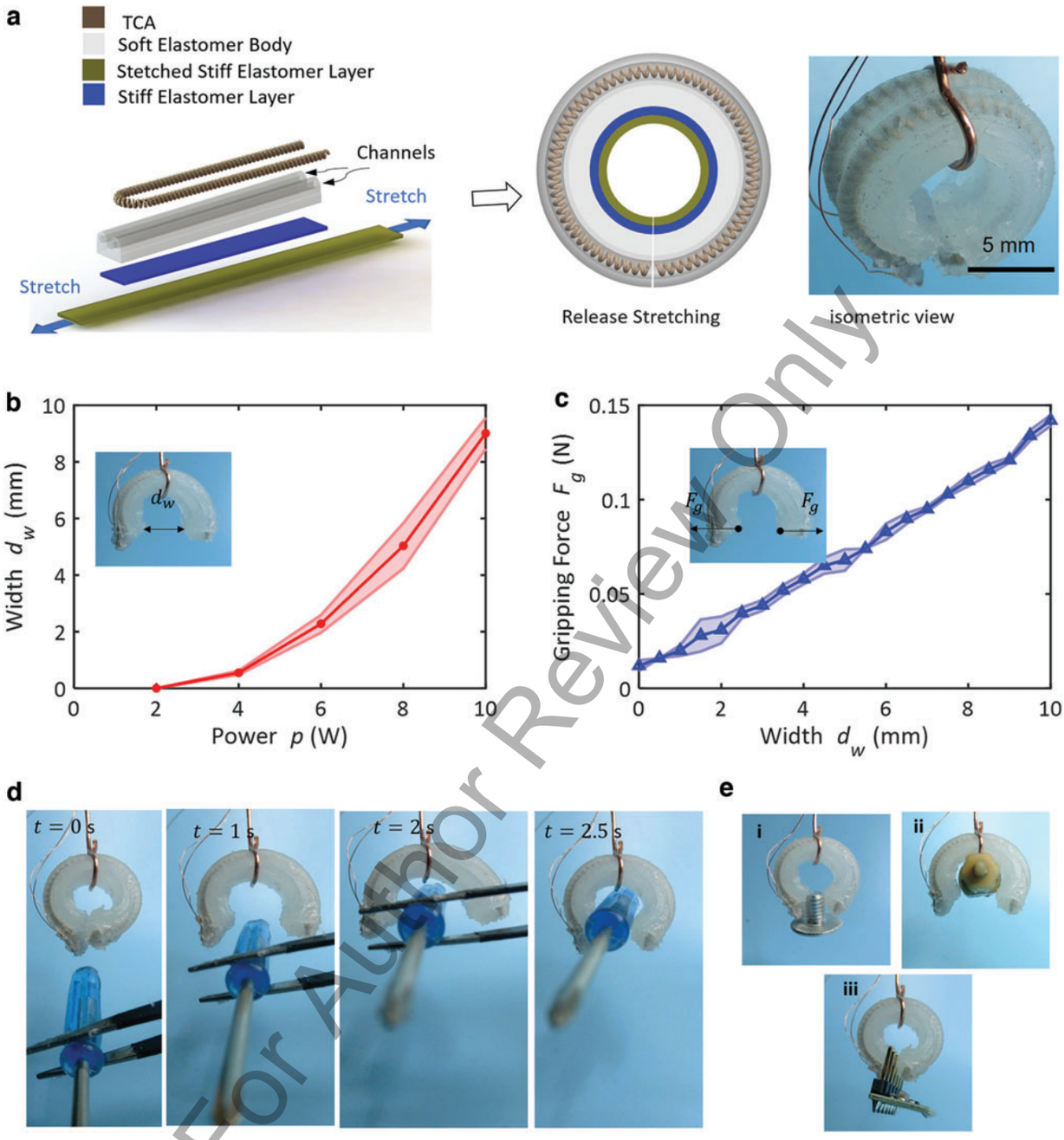

FIG. 5. Two-dimensional bending motion manifested by a gripper which is normally closed and can be opened by actuating an embedded TCA. **(a)** The fabrication schematic of the gripper and an isometric view. **(b)** The opening width of the gripper when different power is applied for 2 s. *Solid lines* indicate the average, and *shaded* regions indicate the standard deviation. The maximum standard deviation is 0.7990 mm. **(c)** The gripping force of the gripper with respect to the opening width. The maximum standard deviation is 0.085 N. **(d)** An example gripping process of a screwdriver. Electricity is applied at $t = 0$ s, the gripper opens wide enough at $t = 2$ s. Finally, at $t = 2.5$ s, the gripper closes and holds a screwdriver. **(e)** Several objects that the gripper can grasp: **(i)** a metal screw, **(ii)** a small DC motor, and **(iii)** a printed circuit board. Color images are available online.

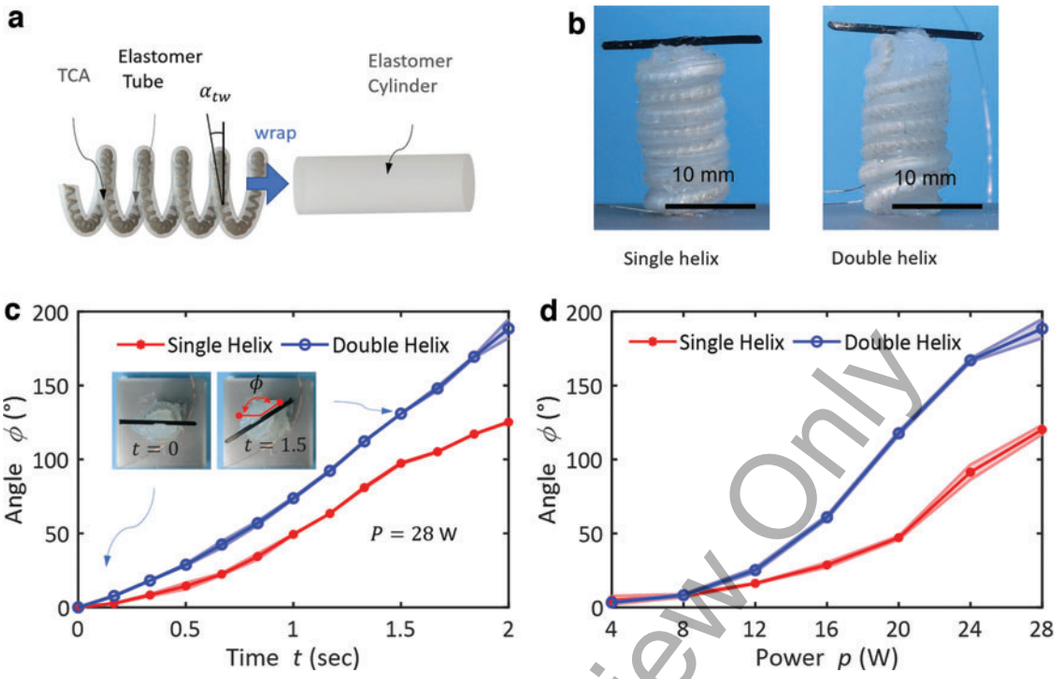

FIG. 6. Twisting motion generated by wrapping a TCA around a cylindrical soft body. **(a)** The schematic of fabricating the twisting module. **(b)** The twisting module with two different wrapping strategies: single helix or a double helix. **(c)** The twisting angles ϕ of the twisting module with respect to time when a power of 28 W is applied. **(d)** The twisting angle of the two modules after applying different power for 2 s. The *lines* indicate the average, and *shaded* regions indicate the standard deviation and the maximum standard deviations are both 6.3640° for **(c, d)**. Color images are available online.

$$p' = [p'_x, p'_y, p'_z]^T$$
$$p = [p_x, p_y, p_z]^T = \frac{L}{\theta}[\sin\gamma(1-\cos\theta),\ \cos\gamma(1-\cos\theta),\ \cos\theta]^T$$

with p' the end position measured in experiments, p the end position represented using γ and θ, and L the length of the module.

Figure 7c shows γ and θ change with respect to time under the same $P_2 = 0.4$ W but different power ratio (P_1/P_2). The bending direction γ (solid lines) and the bending angle θ (dashed lines) increase with respect to time. The slope of θ is more influenced by the power ratio than γ. The increase of θ and γ is almost linear, although γ may decrease a little in the beginning. Figure 7d shows the final values of γ and θ with respect to the power ratio (P_1/P_2) after applying electricity for 2 s. For the bending angle γ with the same P_2, it increases with respect to the power ratio, meaning the module bends more toward TCA1. Also, the values for γ are approximately the same for the two different sets of experiments for the same power ratio, suggesting that it indeed depends on the power ratio instead of the magnitude. For the bending magnitude θ, it increases with respect to the power ratio, similar to the trend for γ. But unlike γ, θ also depends on the magnitude of power. In fact, when the power ratio is the same, the bending magnitude θ for $P_2 = 0.4$ W can be much larger than the case with $P_2 = 0.2$ W. For instance, θ is $\sim 120°$ when $P_1 = 2$ W and $P_2 = 0.4$ W, whereas it is only $\sim 50°$ when $P_1 = 1$ W and $P_2 = 0.2$ W. Note that the applied power is relatively small compared with the input for the twisting module since the 3D bending module has a much smaller bending stiffness than the torsional stiffness. Also, due to the initial curved shape and inaccurate measurement, θ may have a maximum initial error of 10°. The maximum standard deviations for Figure 7c and d are, respectively, 4.53° and 4.49°.

Combination of modular motions: a soft robotic arm

We can combine the three modular motions (2D bending, twisting, and 3D bending) to develop a soft robotic arm: the gripper as a hand, the twisting module as a wrist, and the 3D bending module as an arm. Similar to the human's forearm, the robotic arm can achieve complicated motion and thus functions, for example, to pick and place an object by coordinating the three modules (Fig. 1e, f). In our design, the arm is fabricated by connecting the gripper, the twisting module, and the 3D bending module in serial, with the end of the 3D bending module fixing to a base that can only move up and down (Fig. 8). The total weight of the arm is 6 g, and the dimension is $\sim 10 \times 10 \times 70$ mm.

Figure 8 and Supplementary Video S6 show that the robotic arm can pick up different objects (a screwdriver and a PCB), and place them in different cups. In the process, the object is placed right under the arm with a known orientation. In this case, the wrist needs to first rotate some angles ($\sim 45°$ with an input power of 14 W in Fig. 8a[i] and $\sim 58°$ with input power of 16 W in Fig. 8b[i]) to align the gripper with the object. Then, according to the width of the object, the gripper opens different widths to grip the object (10 W in Fig. 8a[ii] and 8 W in Fig. 8b[ii]). After grasping the object, the wrist will return to its original orientation, and the arm lifts the

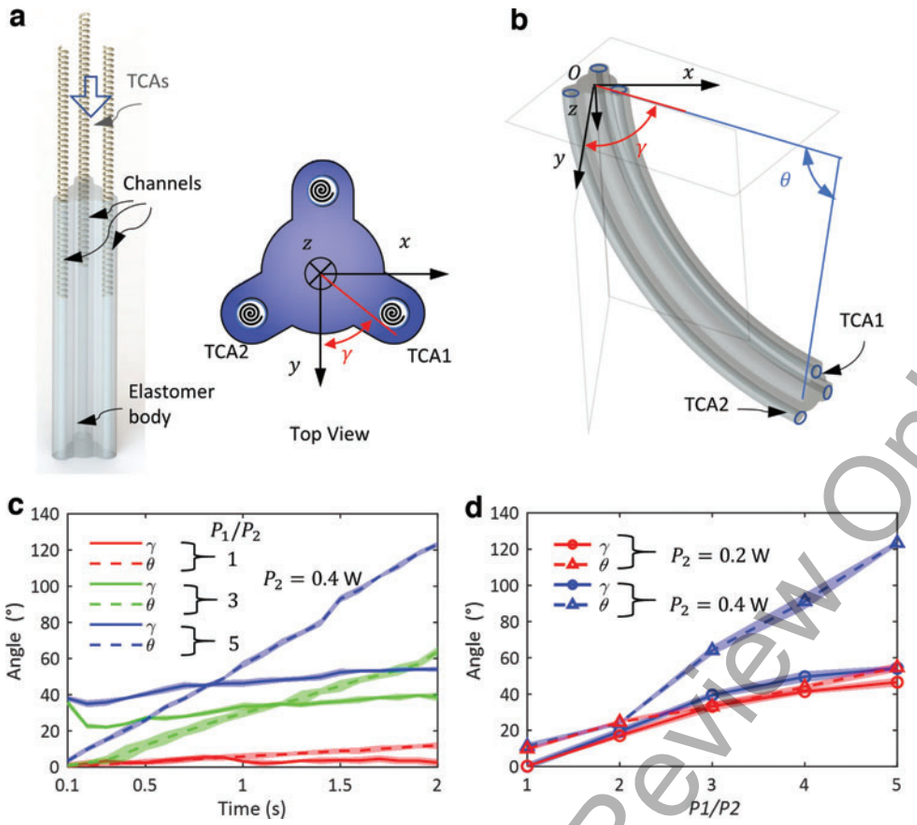

FIG. 7. Three-dimensional bending motion generated by three TCAs placed in parallel in a soft body. **(a)** The schematic to fabricate the 3D bending module with the top view shown on the *right*. **(b)** A three-dimensional schematic showing bending direction γ and the bending angle θ. **(c)** The bending angle and the bending direction with respect to time. **(d)** The bending angle and the bending direction with respect to input power ratio for two cases $P_2 = 0.2$ W and $P_2 = 0.4$ W. For both **(c, d)**, the *lines* indicate the average, and *shaded* regions indicate the standard deviation. The maximum standard deviation of all curves for **(c)** is 4.53°, and for **(d)** it is 4.49°. Color images are available online.

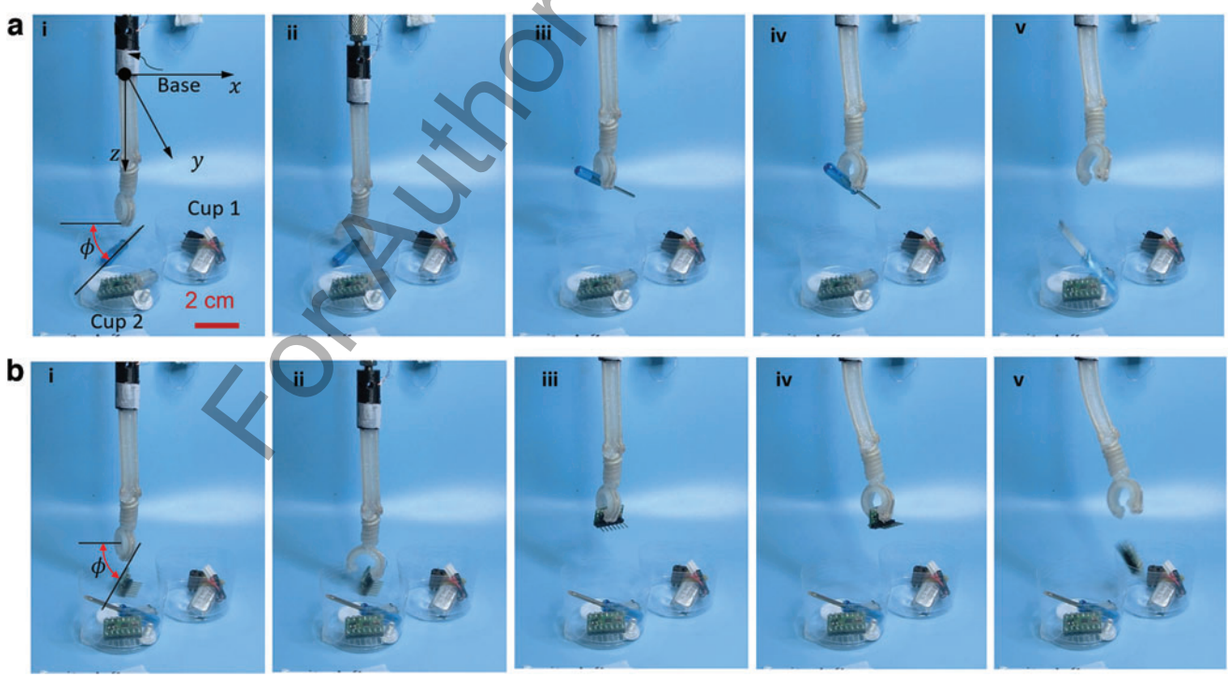

FIG. 8. A soft robotic arm that can perform pick-and-place tasks. **(a-, b–i)**. The object is placed under the gripper. **(ii)** The gripper opens and rotates when the arm approaches the object. **(iii)** The gripper grasps the object and lifts it to a certain height. **(iv)** The arm bends toward the target cup. **(v)** The gripper releases the object into the cup. Color images are available online.

object to some heights by moving up the base in Figure 8a and b(iii). Then, the arm bends toward a desired cup [$P_1 = 0.6$ W, $P_2 = 0.6$ W in Fig. 8a(iv) and $P_1 = 0.2$ W, $P_2 = 0.8$ W in Fig. 8b(iv)]. Finally, the arm releases the object by opening the gripper. Note that the 3D bending module can still bend noticeably (>30°) with the additional weight of the gripper, the twisting module, and the object.

Conclusion

In conclusion, this article presents TCAs with free strokes that are suitable for actuating soft robots. The TCA has an initial state with gaps between coils, so that it can contract without preloading, generating ~50% free strokes that cannot be generated by traditional TCAs. We characterize its static response with respect to temperature and dynamic response with respect to time. The characterization results suggest that a relatively low annealing temperature and a large pitch angle during coiling can generate TCAs that respond faster with larger strokes. When embedding TCAs with free strokes into a soft body to build soft robots, we can achieve versatile, programmed motion, compared with previous work.[19,21,47] We demonstrate individual modules for 2D bending, twisting, and 3D bending motion by properly arranging the TCAs in the soft bodies. By concatenating the individual modules, we build a first ever miniature soft robotic arm actuated by TCAs. We demonstrate pick-and-place operations using the soft robotic arm. More complicated motion can be potentially achieved by arranging TCAs in other desired shapes. However, if the environmental disturbance (temperature, flow condition) is applied, to achieve the precise motion of the soft robots requires a closed-loop control.

Future work will focus on two aspects. First, we will establish both static and dynamic models for both TCAs with free strokes and TCA-actuated soft robots to predict and actively control the resulting motion. This will be accomplished based on our previous efforts on the modeling of traditional TCAs[29] and TCA-actuated soft robots.[24] Note that TCAs with free strokes necessitate new models since our previous models cannot work. Second, we will develop versatile soft robots for locomotion using TCAs with free strokes. Specifically, we will focus on underwater robots since heat dissipation is faster during the recovery process. By properly actuating several TCAs embedded in a soft body, we can potentially accomplish untethered soft robots with versatile motions, which is currently a bottleneck for soft robotics research.[17] Eventually, we envision that the upgraded TCAs can endow a variety of robots, soft or rigid, with large, programmable, and controllable motion in the future.

Author Disclosure Statement

No competing financial interests exist.

Funding Information

This work is partially supported by the National Science Foundation under Grant CNS-1755766.

Supplementary Material

Supplementary Data
Supplementary Table S1
Supplementary Figure S1
Supplementary Figure S2
Supplementary Figure S3
Supplementary Figure S4
Supplementary Figure S5
Supplementary Figure S6
Supplementary Figure S7
Supplementary Figure S8
Supplementary Video SV1
Supplementary Video SV2
Supplementary Video SV3
Supplementary Video SV4
Supplementary Video SV5
Supplementary Video SV6

References

1. Rus D, Tolley MT. Design, fabrication and control of soft robots. Nature 2015;521:467–475.
2. Shepherd RF, Ilievski F, Choi W, *et al.* Multigait soft robot. Proc Natl Acad Sci U S A 2011;108:20400–20403.
3. Calisti M, Giorelli M, Levy G, *et al.* An octopus-bioinspired solution to movement and manipulation for soft robots. Bioinspir Biomim 2011;6:036002.
4. Bartlett NW, Tolley MT, Overvelde JT, *et al.* A 3D-printed, functionally graded soft robot powered by combustion. Science 2015;349:161–165.
5. Gu G-Y, Zhu J, Zhu L-M, *et al.* A survey on dielectric elastomer actuators for soft robots. Bioinspir Biomim 2017; 12:011003.
6. Acome E, Mitchell S, Morrissey T, *et al.* Hydraulically amplified self-healing electrostatic actuators with muscle-like performance. Science 2018;359:61–65.
7. Wehner M, Truby RL, Fitzgerald DJ, *et al.* An integrated design and fabrication strategy for entirely soft, autonomous robots. Nature 2016;536:451.
8. Miriyev A, Stack K, Lipson H. Soft material for soft actuators. Nat Commun 2017;8:596.
9. Wang C, Sim K, Chen J, *et al.* Soft ultrathin electronics innervated adaptive fully soft robots. Adv Mater 2018;30: 1706695.
10. Wang W, Ahn S-H. Shape memory alloy-based soft gripper with variable stiffness for compliant and effective grasping. Soft Robot 2017;4:379–389.
11. Huang X, Kumar K, Jawed MK, *et al.* Chasing biomimetic locomotion speeds: creating untethered soft robots with shape memory alloy actuators. Sci Robot 2018;3:7557.
12. Haines CS, Lima MD, Li N, *et al.* Artificial muscles from fishing line and sewing thread. Science 2014;343:868–872.
13. Tawfick S, Tang Y. Stronger artificial muscles, with a twist. Science 2019;365:125–126.
14. Mirvakili SM, Ravandi AR, Hunter IW, *et al.* Simple and Strong: Twisted Silver Painted Nylon Artificial Muscle Actuated by Joule Heating. In: Electroactive Polymer Actuators and Devices (EAPAD) 2014. Bellingham, WA: International Society for Optics and Photonics, 2014, pp. 90560I.
15. Abbas A, Zhao J. Twisted and Coiled Sensor for Shape Estimation of Soft Robots. In: 2017 IEEE/RSJ International Conference on Intelligent Robots and Systems (IROS), Vancouver, Canada. Piscataway, NJ: IEEE, 2017, pp. 482–487.
16. van der Weijde J, Vallery H, Babuška R. Closed-loop control through self-sensing of a joule-heated twisted and coiled polymer muscle. Soft Robot 2019;6:621–630.
17. Rich SI, Wood RJ, Majidi C. Untethered soft robotics. Nat Electron 2018;1:102.

18. Huang X, Kumar K, Jawed MK, *et al.* Soft electrically actuated quadruped (SEAQ)—Integrating a flex circuit board and elastomeric limbs for versatile mobility. IEEE Robot Autom Lett 2019;4:2415–2422.
19. Tang X, Li K, Liu Y, *et al.* A general soft robot module driven by twisted and coiled actuators. Smart Mater Struct 2019;28:035019.
20. Tang X, Li K, Liu Y, *et al.* A soft crawling robot driven by single twisted and coiled actuator. Sensors Actuat A Phys 2019;291:80–86.
21. Yang Y, Tse YA, Zhang Y, *et al.* A Low-Cost Inchworm-Inspired Soft Robot Driven by Supercoiled Polymer Artificial Muscle. In: 2019 2nd IEEE International Conference on Soft Robotics (RoboSoft), Seoul, Korea. Piscataway, NJ: IEEE, 2019, pp. 161–166.
22. Almubarak Y, Tadesse Y. Twisted and coiled polymer (TCP) muscles embedded in silicone elastomer for use in soft robot. Int J Intell Robot Appl 2017;1:352–368.
23. Wu L, Chauhan I, Tadesse Y. A novel soft actuator for the musculoskeletal system. Adv Mater Technol 2018;3:1700359.
24. Pawlowski B, Sun J, Xu J, *et al.* Modeling of soft robots actuated by twisted-and-coiled actuators. IEEE ASME Trans Mech 2018;24:5–15.
25. Mirvakili SM, Hunter IW. Artificial muscles: mechanisms, applications, and challenges. Adv Mater 2018;30:1704407.
26. Siéfert E, Reyssat E, Bico J, *et al.* Bio-inspired pneumatic shape-morphing elastomers. Nat Mater 2019;18:24.
27. Kotikian A, Truby RL, Boley JW, *et al.* 3D printing of liquid crystal elastomeric actuators with spatially programed nematic order. Adv Mater 2018;30:1706164.
28. Aharoni H, Xia Y, Zhang X, *et al.* Universal inverse design of surfaces with thin nematic elastomer sheets. Proc Natl Acad Sci U S A 2018;115:7206–7211.
29. Abbas A, Zhao J. A Physics Based Model for Twisted and Coiled Actuator. In: 2017 IEEE International Conference on Robotics and Automation (ICRA), Marina Bay Sands, Singapore. Piscataway, NJ: IEEE, 2017, pp. 6121–6126.
30. Haines CS, Li N, Spinks GM, *et al.* New twist on artificial muscles. Proc Natl Acad Sci U S A 2016;113:11709–11716.
31. Li T, Wang Y, Liu K, *et al.* Thermal actuation performance modification of coiled artificial muscle by controlling annealing stress. J Polym Sci B Polym Phys 2018;56:383–390.
32. Yip MC, Niemeyer G. On the control and properties of supercoiled polymer artificial muscles. IEEE Trans Robot 2017;33:689–699.
33. Cho KH, Song MG, Jung H, *et al.* A Robotic Finger Driven by Twisted and Coiled Polymer Actuator. In: Electroactive Polymer Actuators and Devices (EAPAD) 2016, Las Vegas, NV, USA. Bellingham, WA: International Society for Optics and Photonics, 2016, pp. 97981J.
34. Kim K, Cho KH, Jung HS, *et al.* Double helix twisted and coiled soft actuator from spandex and nylon. Adv Eng Mater 2018;20:1800536.
35. Yang SY, Cho KH, Kim Y, *et al.* High performance twisted and coiled soft actuator with spandex fiber for artificial muscles. Smart Mater Struct 2017;26:105025.
36. Kianzad S, Pandit M, Bahi A, *et al.* Nylon Coil Actuator Operating Temperature Range and Stiffness. In: Electroactive Polymer Actuators and Devices (EAPAD) 2015, San Diego, CA, USA. Bellingham, WA: International Society for Optics and Photonics, 2015, pp. 94301X.
37. Masuya K, Ono S, Takagi K, *et al.* Nonlinear Dynamics of Twisted and Coiled Polymer Actuator Made of Conductive Nylon Based on the Energy Balance. In: 2017 IEEE International Conference on Advanced Intelligent Mechatronics (AIM), Munich, Germany. Piscataway, NJ: IEEE, pp. 779–784.
38. Lin H-T, Leisk GG, Trimmer B. GoQBot: a caterpillar-inspired soft-bodied rolling robot. Bioinspir Biomim 2011; 6:026007.
39. Rafie Ravandi A. Characterizing the Behavior of Nylon Actuators and Exploring Methods for Manufacturing Them to Get the Highest Amount of Output. Canada: University of British Columbia, 2018.
40. Cherubini A, Moretti G, Vertechy R, *et al.* Experimental characterization of thermally-activated artificial muscles based on coiled nylon fishing lines. Aip Adv 2015;5: 067158.
41. Huang Y-W, Lee W-S, Chuang Y-F, *et al.* Time-dependent deformation of artificial muscles based on Nylon 6. Mater Sci Eng C 2019;98:445–451.
42. Zhang J, Simeonov A, Yip MC. Three-dimensional hysteresis compensation enhances accuracy of robotic artificial muscles. Smart Mater Struct 2018;27:035002.
43. Konda R, Zhang J. The Effects of Nylon Polymer Threads on Strain-Loading Hysteresis Behavior of Supercoiled Polymer (SCP) Artificial Muscles. In: ASME 2019 Dynamic Systems and Control Conference, Park City, Utah, USA. New York, NY: American Society of Mechanical Engineers Digital Collection.
44. She Y, Li C, Cleary J, *et al.* Design and fabrication of a soft robotic hand with embedded actuators and sensors. J Mech Robot 2015;7:021007.
45. Zhu Z, Meguid S. Elastodynamic analysis of low tension cables using a new curved beam element. Int J Solids Struct 2006;43:1490–1504.
46. Webster III RJ, Jones BA. Design and kinematic modeling of constant curvature continuum robots: a review. Int J Robot Res 2010;29:1661–1683.
47. Sun J, Pawlowski B, Zhao J. Embedded and Controllable Shape Morphing with Twisted-and-Coiled Actuators. In: 2018 IEEE/RSJ International Conference on Intelligent Robots and Systems (IROS), Madrid, Spain. Piscataway, NJ: IEEE, 2018, pp. 5912–5917.

Address correspondence to:
Jianguo Zhao
Department of Mechanical Engineering
Colorado State University
430 North College Avenue
Fort Collins, CO 80523
USA

E-mail: jianguo.zhao@colostate.edu

Supplementary Data

SUPPLEMENTARY VIDEO SV1. A TCA with free strokes overcomes friction.

SUPPLEMENTARY VIDEO SV2. A TCA with free strokes overcomes gravity.

SUPPLEMENTARY VIDEO SV3. Gripper actuated by the TCA with free strokes.

SUPPLEMENTARY VIDEO SV4. Twisting module.

SUPPLEMENTARY VIDEO SV5. 3D bending module.

SUPPLEMENTARY VIDEO SV6. Soft robotic arm.

Supplementary Table S1. The Fabrication Parameter of Twisted-and-Coiled Actuators

No.	α_m	α_n	l_m	l_n	S_f, %	T_a
Type 0-180	11.53	10.8	70	61	5.7	180
Type 1-180	15.57	14.56	94	88	20.4	180
Type 2-180	22.54	18.14	133.5	109	35.7	180
Type 1-200	15.57	15.57	96	96	27.2	200
Type 2-200	22.54	22.54	134	134	48	200